

Differential Information Aided 3-D Registration for Accurate Navigation and Scene Reconstruction

Jin Wu, Shuyang Zhang, Yilong Zhu, Ruoyu Geng, Zhongtao Fu, Fulong Ma and Ming Liu

Abstract—A novel 3-dimensional (3-D) alignment method for point-cloud registration is proposed where the time-differential information of the measured points is employed. The new problem turns out to be a novel multi-dimensional optimization. Analytical solution to this optimization is then obtained, which sets the ground of further correspondence matching using k-D trees. Finally, via many examples, we show that the new method owns better registration accuracy in real-world experiments.

I. INTRODUCTION

A. Background

3-D registration is a popular technology in frontiers of current biomedical imaging, multi-dimensional reconstruction, robotic perception and etc. [1], [2]. It finds out the affine, rigid or non-rigid transformation between two measured point clouds so that multiple 3-D views can be effectively merged. These point cloud measurements typically come from laser scanners, RGB-D cameras, structured light, etc. It also becomes a key technique in attitude determination, localization and mapping using visual measurements [3]–[5]. Potentially, registration is also beneficial to the hand-eye calibration problem [6], [7]. The classical 3-D registration problem between two point frames $\{\mathcal{B}\}$ and $\{\mathcal{R}\}$ can be specified by

$$\arg \min_{\mathbf{R} \in SO(3), \mathbf{T} \in \mathbb{R}^3} \sum_{i=1}^N \|\mathbf{b}_i - \mathbf{R}\mathbf{r}_i - \mathbf{T}\|^2 \quad (1)$$

where \mathbf{R} is the rotation matrix in the 3-D special orthogonal group $SO(3)$ such that $\mathbf{R}^\top \mathbf{R} = \mathbf{I}$, $\det(\mathbf{R}) = 1$; \mathbf{T} is a translation vector and it aligns N points correspondences i.e. $\mathbf{b}_i \in \{\mathcal{B}\}$, $\mathbf{r}_i \in \{\mathcal{R}\}$, $i = 1, 2, \dots, N$ together with the rotation \mathbf{R} . This problem aligns two point sets of $\{\mathbf{b}_i\}$ and $\{\mathbf{r}_i\}$ using a least-square formulation. The target is to find the optimal rotation and \mathbf{R} and translation \mathbf{T} for best point-cloud alignment.

B. Related Work

The problem in (1) has already been solved extensively via the singular value decomposition (SVD, [8]) and eigen-decomposition (EIG, [9]). (1) also plays an important role in point-cloud matching algorithms including iterative closest points (ICP, [10]) and geometric-feature matchers [11]. Problem (1) is quite effective for scenes with large numbers of

points. However, in engineering, matching two point clouds is challenging because the iterative searching is highly non-convex. Extensive efforts have been paid to seek the globally optimal ICP solution, such as Go-ICP [12] and BnB [13]. However, these globally optimal variants are computationally inefficient. Thus, as the point number largely decreases, the complexity of searching increases dramatically. Therefore the registration performance drops accordingly and may even cause failure in engineering use. A key feature existed in these applications is that they are real-time implementations so the laser scanners are moving continuously. It can be noticed that, challenging cases are usually dynamical ones. Therefore more substantial information other than point-cloud measurements should be added for improvement. The time differentiation measurements of successive measured point clouds contains quite fruitful information for 3-D registration. Also, many other sensors like inertial measurement unit (IMU) can provide differential information of attitude via inertial integration [14], [15]. This paper is based on such an idea and proposes a novel 3-D registration method with the aid of time-differential of measured 3-D points. The studied problem is effective for several reasons:

- Previous methods usually solve (1) by approximating an adequate rotation \mathbf{R} via IMU measurements [16], [17]. However, if \mathbf{b}_i and \mathbf{r}_i are biased, the correspondence matching could be failed.
- When incorporating differential information, these biases can be eliminated and therefore will improve registration accuracy. That is to say, the measurements for previous methods are loosely coupled while that of the proposed solution are tightly coupled.
- More time differential information is considered in the new problem. Thus more substantial information will be brought to the studied problem, generating results with higher accuracy.

C. Contributions

The major contributions are

- 1) The differential 3-D registration has been proposed and formulated mathematically for the first time. This allows for a new set of improved registration equations. These equations are highly useful in the presence of multiple conditions.
- 2) Closed-form results are derived according to the presented new equations, which allows computationally efficient computation in real-time.
- 3) We build up multiple k-D trees to conduct simultaneous correspondence matching for points in various

¹J. Wu, S. Zhang, Y. Zhu, R. Geng, F. Ma and M. Liu are with Department of Electronic and Computer Engineering, Hong Kong University of Science and Technology, Clear Water Bay, Hong Kong SAR, China. eelium@ust.hk

²Z. Fu, School of Mechanical and Electronic Engineering, Wuhan Institute of Technology, Wuhan, 430205, China. hustfzt@gmail.com

time instants. The registration results are improved by using well matched point pairs.

D. Outline

The remainder of this paper is structured as follows: Section II presents the theory of proposed differential 3-D registration method. Experimental studies and comparisons are presented in Section III. Finally, concluding remarks are drawn in Section IV.

II. DIFFERENTIAL 3-D REGISTRATION METHOD

A. Rigid Registration

The problem (1) is based on the following ideal case [18]

$$\mathbf{b} = \mathbf{R}\mathbf{r} + \mathbf{T} \quad (2)$$

where the indices of \mathbf{b} and \mathbf{r} are omitted for the sake of convenience. Differentiating (2) with respect to time t gives $\dot{\mathbf{b}} = \mathbf{R}\dot{\mathbf{r}} + \dot{\mathbf{R}}\mathbf{r} + \dot{\mathbf{T}}$, which can be rearranged as

$$\Delta\mathbf{b} - \Delta\mathbf{R}\mathbf{r} - \Delta\mathbf{T} = \mathbf{R}\Delta\mathbf{r} \quad (3)$$

where Δ denotes the incremental item. Here the incremental measurements $\Delta\mathbf{b}$ and $\Delta\mathbf{r}$ can be directly given by the difference of successive outputs. In this paper, the rotational and translational increments are estimated using a windowing-recursive approach (WRA, [19]). WRA can estimate and forecast variables with tiny window size along with few historical data and is proven to be more efficient than traditional interpolation or extrapolation methods. Another kernel task for establishing (3) is to obtain accurate estimates of $\Delta\mathbf{R}$ and $\Delta\mathbf{T}$ so that the registration could be properly refined. Integrating an ultra low-cost IMU into a LIDAR has become a common practice. When combining with IMU, $\Delta\mathbf{R}$ and $\Delta\mathbf{T}$ can be directly computed with inertial navigation mechanisms:

$$\Delta\mathbf{R} = \int_{t \in \mathcal{T}} -[\boldsymbol{\omega}]_{\times} \mathbf{R} dt \quad (4)$$

where $\boldsymbol{\omega}$ is the angular rate and \mathcal{T} denotes the time span between discrete measurements of $\boldsymbol{\omega}$; $[\boldsymbol{\omega}]_{\times}$ represents the skew-symmetric matrix of $\boldsymbol{\omega}$ [20]. The translational increment $\Delta\mathbf{T}$ can be obtained by the IMU preintegration [14]:

$$\begin{aligned} \Delta\mathbf{v} &= \int_{t \in \mathcal{T}} (\mathbf{R}\mathbf{a} - \mathbf{g}) dt \\ \Delta\mathbf{T} &= \mathbf{v}\Delta t + \iint_{t \in \mathcal{T}} (\mathbf{R}\mathbf{a} - \mathbf{g}) dt^2 \end{aligned} \quad (5)$$

in which \mathbf{v} denotes the velocity; \mathbf{g} is the local gravity vector and \mathbf{a} represents the acceleration measured by the IMU with timestamp difference (sampling period) of Δt . However, due to the biases in IMU, integrals in (4) and (5) will suffer from long-term drifts. There are several approaches to compensate for such drift:

- 1) Aid by accelerometer and magnetometer: The rotation drifts can be cancelled by fusing gravitational acceleration and local geomagnetic field [21].

- 2) Aid by zero updates: If the laser scanner is not always in highly dynamical motion, there will be some times when it stops. At such times, the zero angular rate update (ZARU) and zero velocity update (ZUPT) can be invoked for compensation of rotational and translational biases [22].
- 3) Aid by interior information of 3-D laser scan: Like optical flow for 2-D velocity estimation from image sequences, the scene flow can be used for extracting 3-D motions from 3-D measurements. Also, in urban environments, there are many architectures with abundant line and plane features which can be further processed for estimation of rotation and translation [23].
- 4) Aid by visual-laser odometry: Using combination of camera and laser scanner, it is able to measure the scene in 2-D and 3-D simultaneously. Then it is able to conduct the visual-laser odometry for continuous egomotion estimation.

Adding such time-differential information to 3-D registration can double the measured point numbers and thus will enhance the success rate in a degree. The registration problem (1) is transformed into

$$\arg \min_{\mathbf{R} \in SO(3), \mathbf{T} \in \mathbb{R}^3} \left\{ \sum_{i=1}^N \|\mathbf{b}_i - \mathbf{R}\mathbf{r}_i - \mathbf{T}\|^2 + \sum_{i=1}^N \|\tilde{\mathbf{b}}_i - \mathbf{R}\tilde{\mathbf{r}}_i\|^2 \right\} \quad (6)$$

by introducing terms

$$\tilde{\mathbf{b}}_i = \Delta\mathbf{b}_i - \Delta\mathbf{R}\mathbf{r}_i - \Delta\mathbf{T}, \quad \tilde{\mathbf{r}}_i = \Delta\mathbf{r}_i \quad (7)$$

Since the two sub-categories of point clouds in (8) have different scales, we need to equalizing such inconsistency by introducing point decentralization and normalization. The final optimization would be

$$\arg \min_{\mathbf{R} \in SO(3)} \left\{ \sum_{i=1}^N \|\mathbf{c}_i - \mathbf{R}\mathbf{d}_i\|^2 + \sum_{i=1}^N \|\tilde{\mathbf{c}}_i - \mathbf{R}\tilde{\mathbf{d}}_i\|^2 \right\} \quad (8)$$

with

$$\begin{aligned} \mathbf{c}_i &= (\mathbf{b}_i - \bar{\mathbf{b}}) / \|\mathbf{b}_i - \bar{\mathbf{b}}\|, & \mathbf{d}_i &= (\mathbf{r}_i - \bar{\mathbf{r}}) / \|\mathbf{r}_i - \bar{\mathbf{r}}\| \\ \tilde{\mathbf{c}}_i &= (\tilde{\mathbf{b}}_i - \bar{\tilde{\mathbf{b}}}) / \|\tilde{\mathbf{b}}_i - \bar{\tilde{\mathbf{b}}}\|, & \tilde{\mathbf{d}}_i &= (\tilde{\mathbf{r}}_i - \bar{\tilde{\mathbf{r}}}) / \|\tilde{\mathbf{r}}_i - \bar{\tilde{\mathbf{r}}}\| \end{aligned} \quad (9)$$

provided that the centers of mass be given by

$$\bar{\mathbf{b}} = \frac{1}{N} \sum_{i=1}^N \mathbf{b}_i, \quad \bar{\mathbf{r}} = \frac{1}{N} \sum_{i=1}^N \mathbf{r}_i, \quad \bar{\tilde{\mathbf{b}}} = \frac{1}{N} \sum_{i=1}^N \tilde{\mathbf{b}}_i, \quad \bar{\tilde{\mathbf{r}}} = \frac{1}{N} \sum_{i=1}^N \tilde{\mathbf{r}}_i \quad (10)$$

Eventually, the new optimization (8) can be solved by computing the maximum eigenvalue λ_{\max} and its associated eigenvector \mathbf{q} of the following matrix

$$\mathbf{W} = \begin{bmatrix} \text{tr}(\mathbf{B}) & \mathbf{z}^\top \\ \mathbf{z} & \mathbf{B}^\top - \text{tr}(\mathbf{B}) \mathbf{I} \end{bmatrix} \quad (11)$$

such that $\mathbf{W}\mathbf{q} = \lambda_{\max}\mathbf{q}$, where parameters are

$$\mathbf{B} = \frac{1}{N} \left(\sum_{i=1}^N \mathbf{c}_i \mathbf{d}_i^\top + \tilde{\mathbf{c}}_i \tilde{\mathbf{d}}_i^\top \right), \quad \mathbf{z} = \frac{1}{N} \left(\sum_{i=1}^N \mathbf{c}_i \times \mathbf{d}_i + \tilde{\mathbf{c}}_i \times \tilde{\mathbf{d}}_i \right) \quad (12)$$

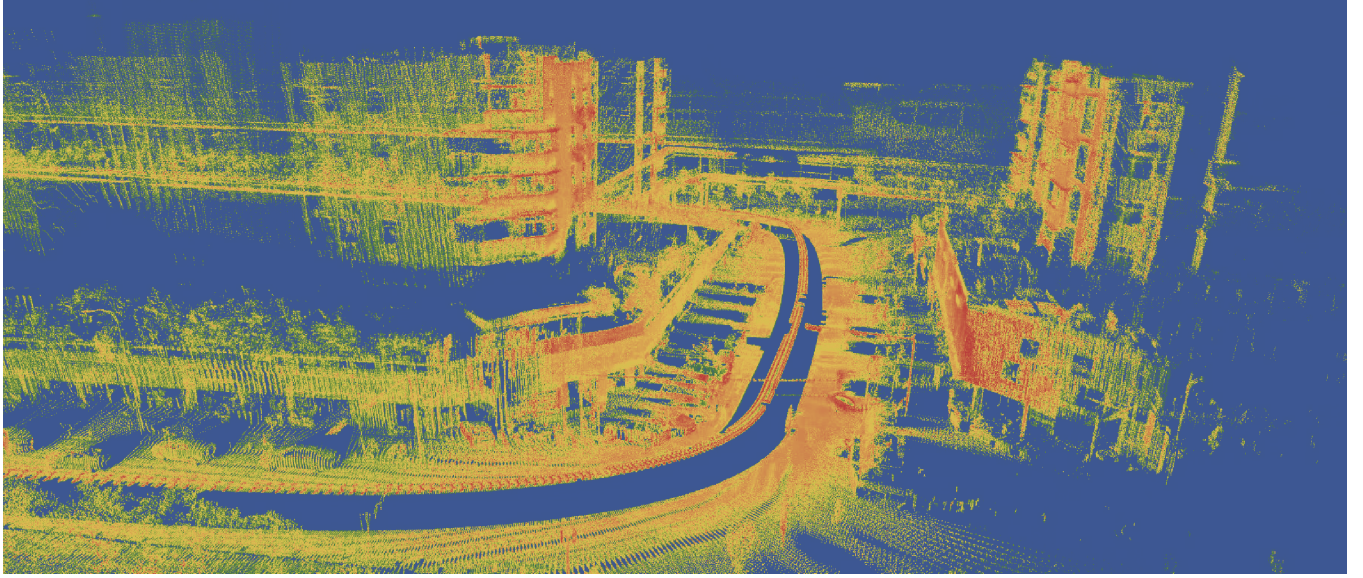


Fig. 1. Reconstructed point-cloud scene using the proposed differential 3-D registration method.

The eigenvector \mathbf{q} is in fact the quaternion and can be converted into a rotation matrix after normalization [24]. A fast closed-form method for extracting such a maximum eigenvalue from \mathbf{W} has also been reported in [25]. When \mathbf{q} is solved from $\mathbf{W}\mathbf{q} = \lambda_{\max}\mathbf{q}$, it is able for us to convert it into rotation matrix \mathbf{R} . Therefore, the translation can be found by $\mathbf{T} = \bar{\mathbf{b}} - \mathbf{R}\bar{\mathbf{r}}$.

B. Correspondence Matching

From successive point cloud measurements, it is hard to obtain $\Delta\mathbf{b}_i$ and $\Delta\mathbf{r}_i$ directly. The reason is that there is no correspondence between $\mathbf{b}_{i,k}$ and $\mathbf{r}_{i,k}$ and finding $\mathbf{b}_{i,k-1}$ and $\mathbf{b}_{i,k}$ also need correspondence matching, where k denotes the time instant. To address this problem, we set up the following matching mechanism

$$\begin{aligned} \arg \min_{\mathbf{R} \in SO(3), \mathbf{T} \in \mathbb{R}^3} & \sum_{i \in \mathcal{B}_k, j \in \mathcal{R}_k} \|\mathbf{b}_{i,k} - \mathbf{R}\mathbf{r}_{j,k} - \mathbf{T}\|^2 + \\ & \sum_{\substack{i \in \mathcal{B}_k, \tilde{i} \in \mathcal{B}_{k-1}, \\ j \in \mathcal{R}_k, \tilde{j} \in \mathcal{R}_{k-1}}} \left\| \frac{\mathbf{b}_{i,k} - \mathbf{b}_{\tilde{i},k-1} - \Delta\mathbf{R}\mathbf{r}_{i,k} - \Delta\mathbf{T} - \mathbf{R}(\mathbf{r}_{i,k} - \mathbf{r}_{\tilde{i},k-1})}{\Delta\mathbf{T} - \mathbf{R}(\mathbf{r}_{i,k} - \mathbf{r}_{\tilde{i},k-1})} \right\|^2 \end{aligned} \quad (13)$$

in which \mathcal{B}_k contains available points for $\mathbf{b}_{i,k}$, $i = 1, 2, \dots$ and \mathcal{R}_k contains available points for $\mathbf{r}_{i,k}$, $i = 1, 2, \dots$; \tilde{i} and \tilde{j} denote the point indices in from previous measurements. (13) forms an new ICP form with correspondence matching from successive point sets in time. To efficiently obtain the correspondences, we use the k-D trees to accelerate the matching. The classical ICP formula employed for comparison is

$$\arg \min_{\mathbf{R} \in SO(3), \mathbf{T} \in \mathbb{R}^3} \sum_{i \in \mathcal{B}_k, j \in \mathcal{R}_k} \|\mathbf{b}_{i,k} - \mathbf{R}\mathbf{r}_{j,k} - \mathbf{T}\|^2 \quad (14)$$

From (14), we may see that the matching process of ICP is much simpler than the proposed one, indicating that the

matching may be ill-posed for some dynamical conditions.



Fig. 2. The UAV platform for aerial laser photographic surveying.

III. EXPERIMENTAL RESULTS

A. Overview

To verify the superiority of the developed algorithm, we use an unmanned aerial vehicle (UAV) platform in Fig. 2 with equipments of onboard rigidly installed IMU (Honeywell) and 3-D laser scanner (Velodyne VLP-16). The time synchronization between the IMU and the laser scanner is conducted via the pulse per-second (PPS) of the real-time kinematic (RTK) global navigation satellite system (GNSS) receiver. The IMU has the sampling rate of 100Hz and the laser scanner's frequency is 20Hz. The system also contains a highly accurate attitude and heading reference system (AHRS) and an accurate integrated navigation system (INS) which provide precision attitude, velocity and position estimation. We use the IMU as an aid to generate time differential data for enhanced point-cloud registration using (8). We pick up a section of the captured data to form a reconstructed point-cloud map using the proposed algorithm. The systematic errors are evaluated using the trajectory

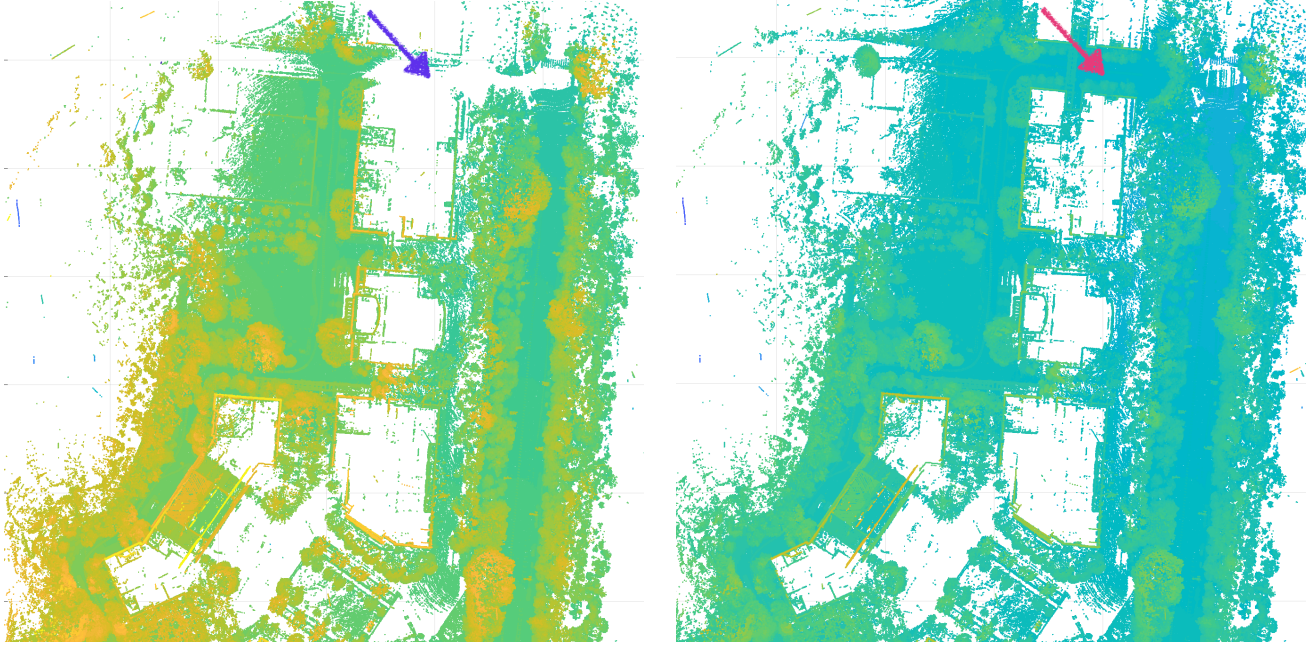


Fig. 3. **Left:** Reconstructed map using IMU-Aided ICP; **Right:** Reconstructed map using the proposed method.

TABLE I
STATISTICAL RESULTS OF REGISTRATION FOR POSE DETERMINATION AND LOCALIZATION OF THE UAV PLATFORM.

Algorithm	Translation Error			Angular Velocity Error		Angular Error	
	$\ T_{\text{est}} - T_{\text{ref}}\ $			$\ (\mathbf{R}_{\text{est}}^\top \dot{\mathbf{R}}_{\text{est}})^\wedge - \boldsymbol{\omega}\ $	$\arccos \{ [\text{tr}(\mathbf{R}_{\text{est}}^\top \mathbf{R}_{\text{ref}}) - 1] / 2 \}$		
	MAE (m)	RMSE (m)	Integral Offset (m)	MAE (rad/s)	RMSE (rad/s)	MAE (rad)	RMSE (rad)
Classical ICP	104.878	52.9346	57.7720	0.69833	0.41421	0.54821	0.39076
IMU – Aided ICP	28.9714	19.4325	21.4767	0.18925	0.09866	0.16301	0.08724
Pure Inertial	93.7082	39.8731	40.2863	—	—	0.32330	0.21987
Proposed	8.67990	2.41562	3.27833	0.16805	0.03219	0.09846	0.03682

MAE : Maximum Absolute Error, RMSE : Root Mean Squared Error, T_{est} : Estimated Translation Vector
 T_{ref} : Reference Translation Vector, \mathbf{R}_{est} : Estimated Rotation Matrix, \mathbf{R}_{ref} : Reference Rotation Matrix

error compared with the ground-truth values from the GNSS receiver. The GNSS signal was healthy due to three installed GNSS antennas so the GNSS trajectory is trustworthy. Typical implementation of k-D tree for correspondence matching can be found in [26]. It should be noted that since more k-D trees are employed, the computational loads for **sequential** k-D trees are higher than that of classical ICP. However, note that all k-D trees can be implemented with **parallelization**. Thus the computational cost of the proposed method for modern multi-core processing computers will not be much higher than that of classical ICP. Rather, since more dynamical measurements are taken into account, the proposed method converges more rapidly than the conventional ICP. For the purpose of comparison, we use ICP and its IMU-aided variant for comparison. The IMU-aided ICP uses the rotation propagating using IMU measurements as a forecast. The mechanisms of inertial attitude/velocity/position propagation are shown in (4) and (5).

B. Results

A test flight of 20-minute duration has been performed using the developed UAV platform. The UAV has been

remotely controlled in an urban scene for 3-D reconstruction. Raw point-cloud measurements are stitched using the results from our proposed method. The reconstructed scene is shown in Fig. 1. The magnified views of one place are presented in Fig. 3. The trajectories using different algorithms are shown in Fig. 4. We also obtained the statistical results of the UAV pose determination and localization, which are shown in Table I. We also test the computational loads of the proposed method and classical ICP, whose results are provided in Table II. In Table II, the maximum absolute error (MAE), root mean squared error (RMSE) are shown. The estimated rotation matrix is \mathbf{R}_{est} and the wedge operation \wedge is the inverse operation of \times such that for the matrix $[\boldsymbol{\omega}]_\times$, we have $([\boldsymbol{\omega}]_\times)^\wedge = \boldsymbol{\omega}$. Therefore, the angular velocity error is $\|(\mathbf{R}_{\text{est}}^\top \dot{\mathbf{R}}_{\text{est}})^\wedge - \boldsymbol{\omega}\|$. The angular error is then defined as $\arccos \{ [\text{tr}(\mathbf{R}_{\text{est}}^\top \mathbf{R}_{\text{ref}}) - 1] / 2 \}$ for describing the difference between the principal axes of \mathbf{R}_{est} and \mathbf{R}_{ref} , where \mathbf{R}_{ref} denotes the reference attitude matrix from the reference system.

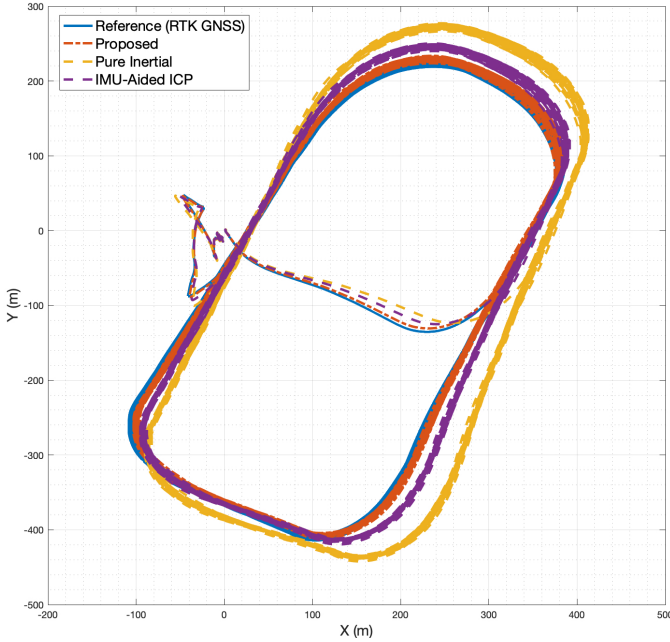


Fig. 4. Trajectories from various registration solutions.

TABLE II
COMPUTATIONAL EFFICIENCY

Algorithms	CPU Load	RAM Occupation
Proposed Method	42.308%	19.923%
Classical ICP	36.833%	13.416%

C. Discussions

From the results presented above, it is able for us to observe the superiority of the proposed method. From Fig. 3, one may see that the proposed method merges more abundant point-cloud scans in the reconstructed scene. The reason is that the proposed method uses multiple k-D trees for correspondence matching of point-cloud points and differential points. Therefore the newly designed matching is more accurate compared with loosely coupled IMU-aided ICP and will match more points for point-cloud merging. From the trajectories using different algorithms shown in Fig. 4, we can see that the pure inertial one owns the worst accuracy while the proposed method has the best precision compared with reference trajectory from RTK GNSS receiver. The IMU-aided ICP ranked at the 2nd place simply because of its loosely coupled nature. The proposed tightly coupled differential approach is capable of eliminating point biases from raw data and thus owns better robustness and accuracy. Therefore the pose determination accuracy and localization accuracy are simultaneously improved, as shown in Table I. As indicated in Section III-A, there are more k-D trees implemented for correspondence matching. However, since all k-D trees are implemented in parallel, the overall computational efficiency is not much higher than classical ICP (see Table II). Nevertheless, since more k-D trees are employed, it is inevitable that more random access memory (RAM) space

must be occupied.

IV. CONCLUSION

In this paper, a new point-cloud registration formulation incorporating the time differential information has been introduced for hybrid registration performance. We show that the time differential information can be easily acquired. Therefore the designed scheme will be practical and easy-to-implement. Through experimental studies, it has been found out that the new formulation can lead to more effective correspondence matching. However, as the dimensions of the measurements have been increased, we inevitably need more space for online processing.

ACKNOWLEDGEMENT

We would like to thank Tencent Robotics X, Shenzhen, China for offering experimental equipments.

REFERENCES

- [1] J. Wu, "Rigid 3D Registration: A Simple Method Free of SVD and Eigendecomposition," *IEEE Trans. Instrum. Meas.*, 2020.
- [2] S. Xu, J. Zhu, Y. Li, J. Wang, and H. Lu, "Effective scaling registration approach by imposing emphasis on scale factor," *Electron. Lett.*, vol. 54, no. 7, pp. 422–424, 2018.
- [3] A. Wan, J. Xu, D. Miao, and K. Chen, "An Accurate Point-Based Rigid Registration Method for Laser Tracker Relocation," *IEEE Trans. Instrum. Meas.*, vol. 66, no. 2, pp. 254–262, 2017.
- [4] J. Du, W. Sheng, and M. Liu, "A human-robot collaborative system for robust three-dimensional mapping," *IEEE/ASME Trans. Mechatronics*, vol. 23, no. 5, pp. 2358–2368, 2018.
- [5] J. Fabian and G. Clayton, "Error Analysis for Visual Odometry on Indoor, Wheeled Mobile Robots With 3-D Sensors," *IEEE/ASME Trans. Mechatronics*, vol. 19, no. 6, pp. 1896–1906, 2014.
- [6] J. Wu, Y. Sun, M. Wang, and M. Liu, "Hand-eye Calibration: 4D Procrustes Analysis Approach," *IEEE Trans. Instrum. Meas.*, 2019.
- [7] J. Wu, M. Liu, C. Zhang, and Z. Zhou, "Correspondence Matching and Time Delay Estimation for Hand-eye Calibration," *IEEE Trans. Instrum. Meas.*, 2020.
- [8] K. S. Arun, T. S. Huang, and S. D. Blostein, "Least-Squares Fitting of Two 3-D Point Sets," *IEEE Trans. Pattern Anal. Mach. Intell.*, vol. PAMI-9, no. 5, pp. 698–700, 1987.
- [9] P. J. Besl and N. D. McKay, "A Method for Registration of 3-D Shapes," *IEEE Trans. Pattern Anal. Mach. Intell.*, vol. 14, no. 2, pp. 239–256, 1992.
- [10] Z. Zhang, "Iterative point matching for registration of free-form curves and surfaces," *Int. J. Comput. Vis.*, vol. 13, no. 2, pp. 119–152, 1994.
- [11] V. Govindu and C. Shekhar, "Alignment using distributions of local geometric properties," *IEEE Trans. Pattern Anal. Mach. Intell.*, vol. 21, no. 10, pp. 1031–1043, 1999.
- [12] J. Yang, H. Li, D. Campbell, and Y. Jia, "Go-ICP: A Globally Optimal Solution to 3D ICP Point-Set Registration," *IEEE Trans. Pattern Anal. Mach. Intell.*, vol. 38, no. 11, pp. 2241–2254, 2016.
- [13] A. Parra Bustos, T. J. Chin, A. Eriksson, H. Li, and D. Suter, "Fast Rotation Search with Stereographic Projections for 3D Registration," *IEEE Trans. Pattern Anal. Mach. Intell.*, vol. 38, no. 11, pp. 2227–2240, 2016.
- [14] C. Forster, L. Carlone, F. Dellaert, and D. Scaramuzza, "On-manifold preintegration for real-time visual - Inertial odometry," *IEEE Trans. Robot.*, vol. PP, no. 99, pp. 1–21, 2016.
- [15] J. Wu, "MARG Attitude Estimation Using Gradient-Descent Linear Kalman Filter," *IEEE Trans. Autom. Sci. Eng.*, 2020.
- [16] F.aghili and C.-Y. Su, "Robust Relative Navigation by Integration of ICP and Adaptive Kalman Filter Using Laser Scanner and IMU," *IEEE/ASME Trans. Mechatronics*, vol. 21, no. 4, pp. 2015–2026, 2016.
- [17] J. Zhang and S. Singh, "Low-drift and real-time lidar odometry and mapping," *Auton. Robots*, vol. 41, no. 2, pp. 401–416, 2017.
- [18] G. Chang, "Total least-squares formulation of Wahba's problem," *Electron. Lett.*, vol. 51, no. 17, pp. 1334–1335, 2015.

- [19] Z. Zhou, Y. Shen, and B. Li, “A windowing-recursive approach for GPS real-time kinematic positioning,” *GPS Solut.*, vol. 14, no. 4, pp. 365–373, 2010.
- [20] M. Namvar and F. Safaei, “Adaptive compensation of gyro bias in rigid-body attitude estimation using a single vector measurement,” *IEEE Trans. Automat. Contr.*, vol. 58, no. 7, pp. 1816–1822, 2013.
- [21] J. Wu, Z. Zhou, J. Chen, H. Fourati, and R. Li, “Fast Complementary Filter for Attitude Estimation Using Low-Cost MARG Sensors,” *IEEE Sens. J.*, vol. 16, no. 18, pp. 6997–7007, 2016.
- [22] A. R. Jiménez Ruiz, F. Seco Granja, J. C. Prieto Honorato, and J. I. Guevara Rosas, “Accurate pedestrian indoor navigation by tightly coupling foot-mounted IMU and RFID measurements,” *IEEE Trans. Instrum. Meas.*, vol. 61, no. 1, pp. 178–189, 2012.
- [23] J. Zhang, M. Kaess, and S. Singh, “A real-time method for depth enhanced visual odometry,” *Auton. Robots*, vol. 41, no. 1, pp. 31–43, 2017.
- [24] J. Wu, “Optimal Continuous Unit Quaternions from Rotation Matrices,” *J. Guid. Control. Dyn.*, vol. 42, no. 4, pp. 919–922, 2019.
- [25] J. Wu, Z. Zhou, B. Gao, R. Li, Y. Cheng, and H. Fourati, “Fast Linear Quaternion Attitude Estimator Using Vector Observations,” *IEEE Trans. Autom. Sci. Eng.*, vol. 15, no. 1, pp. 307–319, 2018.
- [26] A. Kosuge, K. Yamamoto, Y. Akamine, and T. Oshima, “An soc-fpga-based iterative-closest-point accelerator enabling faster picking robots,” *IEEE Trans. Indust. Elect.*, 2020.